Meteorol Atmos Phys (2013) 122:19–32
DOI 10.1007/s00703-013-0275-3

ORIGINAL PAPER

Impact of ocean warm layer thickness on the intensity of hurricane Katrina in a regional coupled model

Hyodae Seo · Shang-Ping Xie

Received: 30 November 2012 / Accepted: 20 August 2013 / Published online: 3 September 2013

Abstract The effect of pre-storm subsurface thermal structure on the intensity of hurricane Katrina (2005) is examined using a regional coupled model. The Estimating Circulation and Climate of Ocean (ECCO) ocean state estimate is used to initialize the ocean component of the coupled model, and the source of deficiencies in the simulation of Katrina intensity is investigated in relation to the initial depth of 26 °C isotherm (D26). The model underestimates the intensity of Katrina partly due to shallow D26 in ECCO. Sensitivity tests with various ECCO initial fields indicate that the correct relationship between intensity and D26 cannot be derived because D26 variability is underestimated in ECCO. A series of idealized experiments is carried out by modifying initial ECCO D26 to match the observed range. A more reasonable relationship between Katrina's intensity and pre-storm D26 emerges: the intensity is much more sensitive to D26 than to sea surface temperature (SST). Ocean mixed layer process plays a critical role in modulating inner-core SSTs when D26 is deep, reducing mixed layer cooling and lowering the center pressure of the Katrina. Our result lends strong support to the notion that accurate initialization of pre-storm subsurface thermal structure in prediction models is critical for a skillful forecast of intensity of Katrina and likely other intense storms.

Responsible editor: J. Fasullo.

H. Seo (✉)
Physical Oceanography Department, Woods Hole Oceanographic Institution, 266 Woods Hole Road, MS#21, Woods Hole, MA 02543, USA
e-mail: hseo@whoi.edu

S.-P. Xie
Scripps Institution of Oceanography, University of California San Diego, 9500 Gilman Drive # 0206, La Jolla, CA 92093, USA

1 Introduction

The amount of upper ocean thermal energy, hereafter referred to as the upper ocean heat content (UOHC, Leipper and Volgenau 1972), is the primary energy source term for the development of hurricanes. The UOHC is determined by the temperature integrated from the surface to the depth of the 26 °C isotherm (D26), i.e., $\mathrm{UOHC}(x,y) = \rho_o C_p \int_{D26}^{sfc} (T(x,y,z) - 26)\,dz$, where, D26 represents an approximate thickness of the upper ocean warm layer, ρ_o is the density of seawater (1,025 kg m^{-3}) and C_p is the specific heat at constant pressure (4×10^3 J kg^{-1} $°C^{-1}$). The reference temperature, 26 °C, is the typical near-surface air temperature in the subtropical atmosphere (Price 2009). Since tropical cyclones mostly form over surface water with temperature of 26 °C or higher, $T(\mathrm{sfc}) - 26$ °C, the upper bound of the integration, represents a thermal disequilibrium between the air and sea, resulting in an enthalpy transfer to the hurricane. Consequently, the higher equivalent potential temperature (θ_e) in the lower atmosphere reduces the storm's central pressure (Kleinschmidt 1951; Riehl and Malkus 1961; Riehl 1963).

During the typical hurricane seasons in the Gulf of Mexico (GoM), the temperatures at the sea surface and subsurface are rather distinct, making it difficult to detect the latter from the former (e.g., Goni and Trinanes 2003). As suggested from the recent studies, information on the pre-storm spatial distribution of the subsurface thermal structure has an important implication to the prediction of storm intensity, whereby in situ ocean mixed layer (OML) dynamics bridge these two (e.g., Halliwell et al. 2008; Lin

et al. 2012). A strengthening storm produces the self-induced cooling of inner-core sea surface temperature (SST) via turbulent mixing and upwelling (e.g., Chang and Anthes 1978, 1979; Sutyrin and Khain 1984; Sanford et al. 1987, 2007; Price et al. 1994; Schade and Emanuel 1999; Bender and Ginis 2000; Shay and Uhlhorn 2008), leading to a negative feedback to the storm intensity (Price 1981; Emanuel 1999; Cione and Uhlhorn 2003). Here, a pre-existing ocean thermal structure is important for the extent to which OML processes modulate the amplitude of this negative feedback; when a hurricane propagates over the region of a deeper D26, the reduced OML cooling further increases θ_e, allowing the storm to intensify further.

The UOHC feedback for storm intensity has been extensively studied in the literature. Shay et al. (2000), for example, reported that the observed ocean cooling by the Hurricane Opal (1995) was only 0.5–1 °C over the warm core ring (WCR) with deeper and warmer thermal structure, while over the ambient Gulf Common Water with the lower heat content, the cooling was greater than 2–3 °C. Sensitivity studies with a fully coupled model by Hong et al. (2000) confirmed that the interaction of Opal with the WCR resulted in an additional 60 % of the intensification compared to the case without such a thermodynamic feature. A similar conclusion was reached for the typhoon Maemi (2003) in the western Pacific using a simple hurricane–ocean coupled model by Wu et al. (2007); the transient ocean warm eddy represents ~64 % of the intensification (Lin et al. 2005). These studies underscore the importance of the pre-existing subsurface ocean thermal structure to the storm intensity via in situ OML dynamics.

Hurricane Katrina (2005) exhibited similar evolution. Scharroo et al. (2005) showed from satellite altimetry data that Katrina underwent a rapid deepening by >50 hPa in sea level pressure (SLP) in less than 12 h over a WCR. Through atmosphere-only sensitivity simulations, by contrast, Sun et al. (2006) suggested that Katrina would have been intensified by 10 hPa if the domain-wide SST were raised by 2 °C, arguing that SST was more important for the rapid intensification. Further numerical studies using coupled models are necessary to quantify the relative importance of ocean subsurface structure and SST in Katrina's rapid intensification.

This study assesses the impact of such pre-storm ocean thermal structures on the intensity of hurricane Katrina in a moderate resolution (0.13°) regional coupled model. The resolution of the model is not high enough to simulate the true intensity of a tropical cyclone (c.f., Murakami et al. 2012), but it has skills in intensity change in response to environmental parameters as discussed in a number of studies (e.g., Hong et al. 2000; Knutson et al. 2007; Zhao et al. 2009). Based on a large number of sensitivity tests, here we attempt to identify the cause for weak intensity response of Katrina to the subsurface thermal fields in ECCO, and to gain insights into the way the ECCO ocean state estimation can be improved for the purpose of hurricane simulation. Note that the effect of spatial variations in subsurface structure has been previously studied (e.g., Hong et al. 2000; Emanuel et al. 2004; Goni et al. 2009). While the hurricane Katrina is chosen as the target case, the results of this study, based on the idealized sensitivity experiments, could be applied to other hurricane case since the OML process is not unique to Katrina.

The paper is organized as follows. Section 2 introduces the regional coupled model and discusses the experimental setup. Section 3 illustrates the evolution of the ocean–atmosphere system to the hurricane passage. Sections 4 and 5 explore the sensitivity of Katrina's intensity to the ocean initial conditions with varying ocean states, yielding the major conclusion of this study. Section 6 is a summary and discusses implications of the results for hurricane prediction.

2 Model

The regional coupled model used in this study is the Scripps Coupled Ocean–Atmosphere Regional (SCOAR) model (Seo et al. 2007). SCOAR couples the two well-known regional models, the Regional Spectral Model (RSM, Juang and Kanamitsu 1994) for the atmosphere and the Regional Ocean Modeling System (ROMS, Haidvogel et al. 2000; Shchepetkin and McWilliams 2005) for the ocean. These RSM and ROMS are coupled at the 1-hourly frequency via the bulk formula for wind stress and heat flux (Fairall et al. 1996). More details can be found in Seo et al. (2007). The horizontal resolutions of RSM and ROMS are identically 0.13° with the matching land–sea mask and coastline. A model of this resolution would underestimate the storm intensity. Our question is what affects storm intensity in a relative, not absolute, sense. ROMS uses 30 vertical layers in this study, with approximately 14 layers in the upper 100 m and roughly 4–8 layers between the base of the mixed layer and the main thermocline.

RSM is initialized from the NCEP/Department of Energy (DOE) Reanalysis 2 (NCEP2, Kanamitsu et al. 2002) at 00Z 26 August 2005 and is integrated for 5 days until 00Z 31 August 2005 with the NCEP2 lateral boundary conditions for prognostic fields. RSM utilizes the Kain–Fritsch convective parameterization scheme (Kain and Fritsch 1993; Kain 2004). The spectral nudging technique (Yoshimura and Kanamitsu 2008) is adopted on the zonal scale greater than 3,000 km in the atmosphere, comparable to the domain size as shown in Fig. 1. This interior nudging is essentially the same technique as in Knutson et al. (2007), which is intended to keep the large-scale

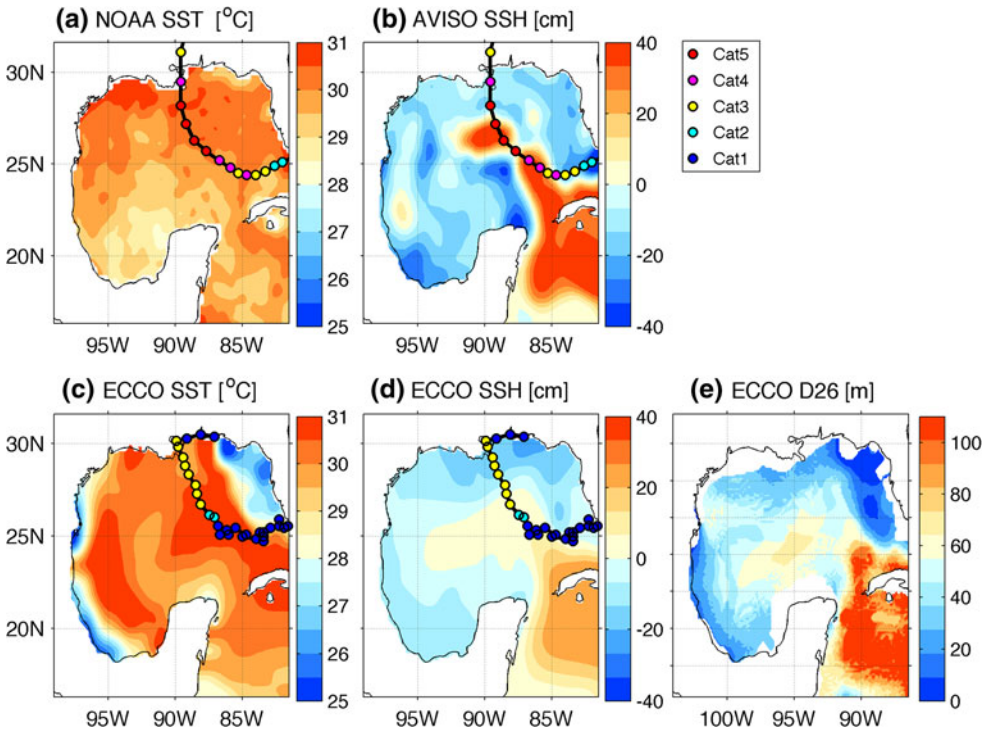

Fig. 1 *Top* **a** sea surface temperature (SST, °C) and **b** sea surface height (SSH, cm) on 26 August 2005 derived from the NOAA Optimum Interpolation SST Analysis and the Archiving, Validation, and Interpretation of Satellite Oceanographic (AVISO) merged satellite data. *Bottom* as in *top* but from **d**–**f** 10-daily ECCO ocean state estimation, in addition to **e** the depth of 26 °C isotherm (D26, m) estimated from ECCO. 10-daily ECCO data are linearly interpolated to obtain the fields on 26 August 2005. The observed (**a**, **b**) and simulated (**c**, **d**) tracks of Katrina are overlaid with the *color circles* indicating the Saffir–Simpson hurricane scale. While the model output is 1-hourly, the tracks shown are 3-hourly for clarity of illustration

environment of the downscaled field consistent with the prescribed background field, while the small-scale process like tropical cyclones can freely evolve and interact with the ocean.

The initial and boundary conditions for ROMS are derived from the Estimating Circulation and Climate of Ocean (ECCO) ocean state estimates (kf066b, http://ecco.jpl.nasa.gov) on 1°×1° grid at a 10-day interval. ROMS is initialized from the 26 August 2005 ocean condition obtained by a linear interpolation between 22 August and 1 September.

For the data analysis and model validation, we will be also using the following datasets. Daily SST data are obtained from the NOAA Optimum Interpolation (OI) SST Analysis (http://www.ncdc.noaa.gov/oa/climate/research/sst/oi-daily-information.php), which incorporates the SSTs measured by the Advanced Very High Resolution Radiometer satellites (Reynolds et al. 2007). Sea surface height (SSH) data are obtained from the Archiving, Validation, and Interpretation of Satellite Oceanographic (AVISO) merged satellite data (http://www.aviso.oceanobs.com). We will also use the Simple Ocean Data Assimilation (SODA) analysis with monthly temporal and 0.5° horizontal resolutions (Carton et al. 2000) to facilitate the validation of ECCO against the AVISO data.

Figure 1 shows the model domain and compares the initial conditions used in the ocean model for SST, SSH, and D26 estimated from ECCO to those from the NOAA OI SST and the AVISO SSH. Observations show the uniformly warm SSTs exceeding 31 °C over the northern Gulf and the intrusion of the Loop Current (LC) and the WCR in the central north Gulf (90°W, 27°N). ECCO does not well represent the intrusion of LC and the presence of WCR. The vertical cross-section of ocean temperature as a function of depth along 26°N across the LC bulge (Fig. 2) shows that the seasonal (D26) and permanent (D20) thermoclines are generally flatter and shallower in ECCO compared to the observations (e.g., Shay 2009), leading to a weak spatial variation in D26 associated with LC/WCR. ECCO SST is generally too warm in GoM except near the coast (Fig. 1c). This discrepancy in SST may contribute to the errors in hurricane intensity.

3 Simulated storm intensity and ocean mixed layer processes

Using the ECCO oceanic state estimates of temperature, salinity, SSH, velocity fields on 26 August 2005 as an initial condition, the SCOAR model was run for the period

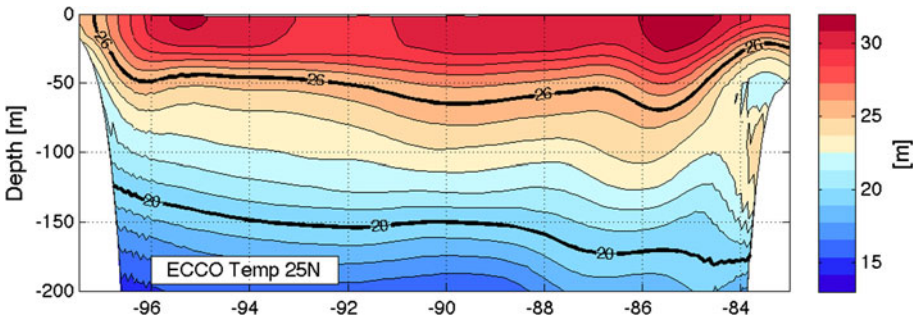

Fig. 2 Temperature cross-sections along 25°N from ECCO on 26 August 2005. The contour interval is 1 °C, with the 26 and 20 °C isotherms indicated as *thick curves*

of a rapid intensification of Katrina. In observations (Fig. 1a, b), Katrina first intensified when it propagated over the LC at 86°W, 24°N with high SST, deep D26, high UOHC and high SSH on 27 August. Katrina then moved over the WCR on 28–29 August (Goni and Knaff 2009), and rapidly intensified into a category 5 hurricane. The simulated hurricane follows this observed rapid intensity change (Fig. 3), although the simulated intensity is weak compared to the observed one. The simulated wind speed, for example, does not exceed 40 m s^{-1}, while the NOAA Hurricane Surface Wind Analysis (H*Wind, Powell et al. 1996) indicates a much wider distribution of wind speed reaching the maximum value of ~98 m s^{-1} (not shown). The simulated weak intensity is somewhat expected since the 0.13° resolution atmospheric model is not sufficient to capture the hurricane inner-core dynamics and eye-wall processes responsible for dramatic changes in storm intensity (Willoughby and Black 1996). Weaker simulated intensity is also attributable to the lack of hurricane initialization scheme in the atmosphere (e.g., Fujihara 1980; Wang 1998). We note that our goal is to identify, from a number of sensitivity tests, factors in the ECCO initial ocean state that modulate the storm intensity via the OML dynamics (Sects. 4, 5).

The simulated intensity of Katrina reaches the maximum intensity 12 h later than in the observed data at 12Z 28 August. The center of the storm in this study is detected as the location of the minimum SLP based on the 1-hourly model outputs, which is compared with the best-track data based on the Atlantic Hurricane Database Re-analysis Project (HURDAT, http://www.nhc.noaa.gov/pastall.shtml#hurdat). The simulated time of landfall is 06Z 29 August, roughly the same as in the observed landfall. The best-track data show a ~90 hPa deepening of the center pressure from 26 August until landfall, while the model shows only a ~50 hPa deepening. The modeled storm dissipates at roughly the same rate upon landfall as in observations.

Figure 4 describes the evolution of the oceanic and atmospheric states associated with the passage of the simulated Katrina at 12-hourly increments. The heavy precipitation exceeding 1,000 mm day^{-1} can be seen at 00Z 29 August, which is stronger to the right of the track. The near-surface wind fields (vectors in the left panel of Fig. 4) also have a highly asymmetric spatial distribution with the rightward bias. From 00Z 29 August, the simulated Katrina begins to produce a cold wake in the SST field, which is again more pronounced to the right of the track, where the wind speed is greater, and the vertical shear of horizontal currents is stronger (Price 1981). SSH (D26 and UOHC likewise, figures not shown) exhibits a dramatic reduction after the passage of Katrina. There is a storm surge propagating westward as coastally trapped waves, reaching >2.5 m upon landfall, as shown from the Hurricane Ivan (Zamudio and Hogan 2008). In the trail of Katrina, large-amplitude (>2 ms^{-1}) clockwise-rotating near-inertial surface currents are excited, again stronger on the right side of the track (Zedler et al. 2002).

The rightward biased response of the mixed layer temperature and currents is due to the asymmetry in turning direction of the wind stress in the ocean surface in a quiescent ocean (Price 1981; Price et al. 1994). In the LC

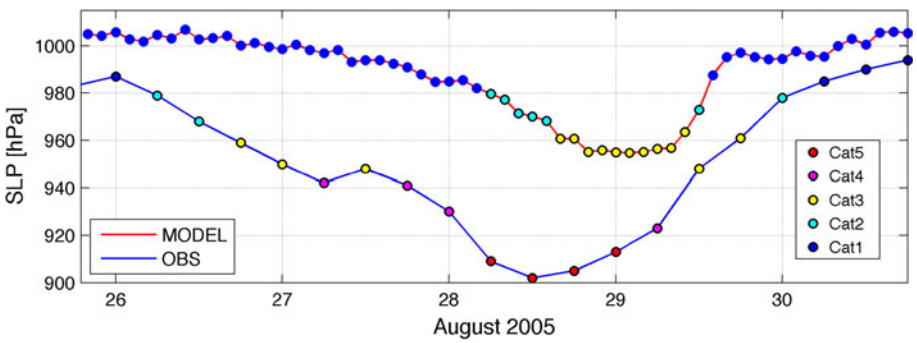

Fig. 3 Time series of the minimum sea level pressure in 26–31 August 2005 from the best-track data (*blue* 6-hourly) and the model (*red* 2-hourly)

region where the pre-existing background geostrophic current is intense (1–2 m s^{-1}), the horizontal advection also significantly affects the upwelling response to the hurricane (e.g., Jacob et al. 2000). In both cases, to the right of the storm center, the stronger shear-driven mixing is due to the resonance between wind and current. The stability of water column in the presence of vertical shear of horizontal current is evaluated by the Richardson number (Ri), defined as $\mathrm{Ri} = N^2/S^2$, where $N^2 = -g/\rho\ (\partial\rho/\partial z)$ denotes buoyancy frequency $S^2 = (\partial u/\partial z)^2 + (\partial v/\partial z)^2$ represents the vertical shear of horizontal currents. ρ denotes the sea water density, g the gravitational acceleration, and u and v the zonal and meridional currents.

Figure 5 shows the time series of N^2, S^2 and Ri at two locations, 86.8°W, 26.5°N, and 89.7°W, 26.5°N, which are located $2R_{\max}$ west and east of the reference point, respectively. The center of Katrina passes this reference point at 18Z 28 August. $R_{\max}$ denotes the radius of simulated maximum wind speed ($\sim$86 km). Prior to the storm passage, the strongest stratification is found at 30–50 m depth in the both east and west. The signal of growing shear (S^2) is found to be nearly 1 IP, where IP stands for the inertial period (26.9 h at this location), prior to the storm passage. After the storm passage, both S^2 and N^2 exhibit oscillations, only in the east, with a periodicity of 1.5 IP, somewhat longer than the typical near-inertial period. The frequency of the inertial waves in the presence of background geostrophic shear is shifted from f to $f_e = f + \zeta/2$, where f is the local Coriolis frequency, ζ the background geostrophic vorticity and f_e the effective Coriolis frequency (e.g., Weller 1982; Kunze 1985). A slightly longer inertial period in the model compared to the estimates from the observations thus implies that, at this particular location (89.7°W, 26.5°N), the pre-storm background vorticity was perhaps more anticyclonic. However, since the ocean model simulation integrates only until $t < 2$IP in the post-storm condition, it is difficult to examine the detailed evolution of near-inertial oscillation in the hurricane wake. During $t < 2$IP in post-storm condition, the depth of the maximum N^2 represented in ECCO is located overly shallow compared to the observations implied from Jaimes and Shay (2009, 2010), while the magnitude is generally reasonable. Despite the large S^2 in the wake due to the storm passage, Ri is never lowered below the criticality (0.25, black curves) below the 30 m depth. The simulated vertical velocity is of $\sim$0.1 m s^{-1} (not shown), an order smaller than the estimate from the observations (Jaimes and Shay 2009, their Fig. 11). This underestimation of vertical velocity is in part due to weaker Ekman pumping velocity associated with the weaker simulated storm intensity and the coarse resolution of the model.

Overall, while some general features associated with the hurricane passage are qualitatively realistic, the several deficiencies in ECCO, such as the overly stratified upper ocean and underestimated spatial structures of D26 associated with LC/WCR, result in a weak mixed layer process. The subsequent feedback to the intensity of Katrina via altered inner-core SST would thus be weak with the ECCO ocean initial condition. This is assessed in the following section with a different set of ocean initial conditions.

4 Oceanic contribution to the hurricane intensity

In this section, 15 more simulations are performed with different ECCO initial fields to assess the extent to which the different ocean thermal conditions and stratification are associated with the intensity response of Katrina. In the ocean component of the coupled model, the initial ocean state on 26 August 2005 is replaced by that of the same date but in different years from 1993 to 2008 from ECCO. The ocean lateral boundary conditions are also changed accordingly. Since the identical initial and boundary conditions are used for the atmosphere, the difference in intensity in hurricane is identified as due to the different oceanic contribution via initial thermal structure and the in situ OML process that modulates the along-track SSTs as illustrated below.

The top panel of Fig. 6 shows the SLP difference in select equivalent ocean years (1996, 2000, 2004, and 2008) compared to 2005 [i.e., SLP(year)–SLP(2005)] at 74 h after the initialization (02Z 29 August). Also shown in gray curves are the storm tracks in each year. The simulated tracks are insensitive to ocean states; they are primarily controlled by the large-scale atmospheric conditions in the model. However, there are noticeable differences in intensity. All the experiments show generally weaker intensity (higher SLP) compared to the case of 2005. The time-series in difference of along-track SLP in these 4 years compared to the 2005 case (Fig. 7a) also suggests that the SLP of all 4 years are higher throughout the integrations with differences reaching up to +6 hPa.

Figure 6 also compares the differences in initial SST (2nd row) and initial D26 (3rd row) of each year with those in 2005. Figure 7b, c shows the along-track variations in SST and D26. The four years shown in Fig. 6 exhibit generally lower basin-wide initial SST compared to that in 2005, with the difference reaching >2 °C. The initially colder SSTs in these years tend to remain colder during the forced stage (Fig. 7b). Both conditions would favor weaker intensity as seen in these years. The initial D26s tend to be deeper in those years, however, which also remain deeper than the 2005 case between 00Z 28 August and the landfall (Fig. 7c). Since translation speeds, U_h, of the simulated storms are not significantly different among the runs (not shown), we hypothesize that the apparent contradiction of

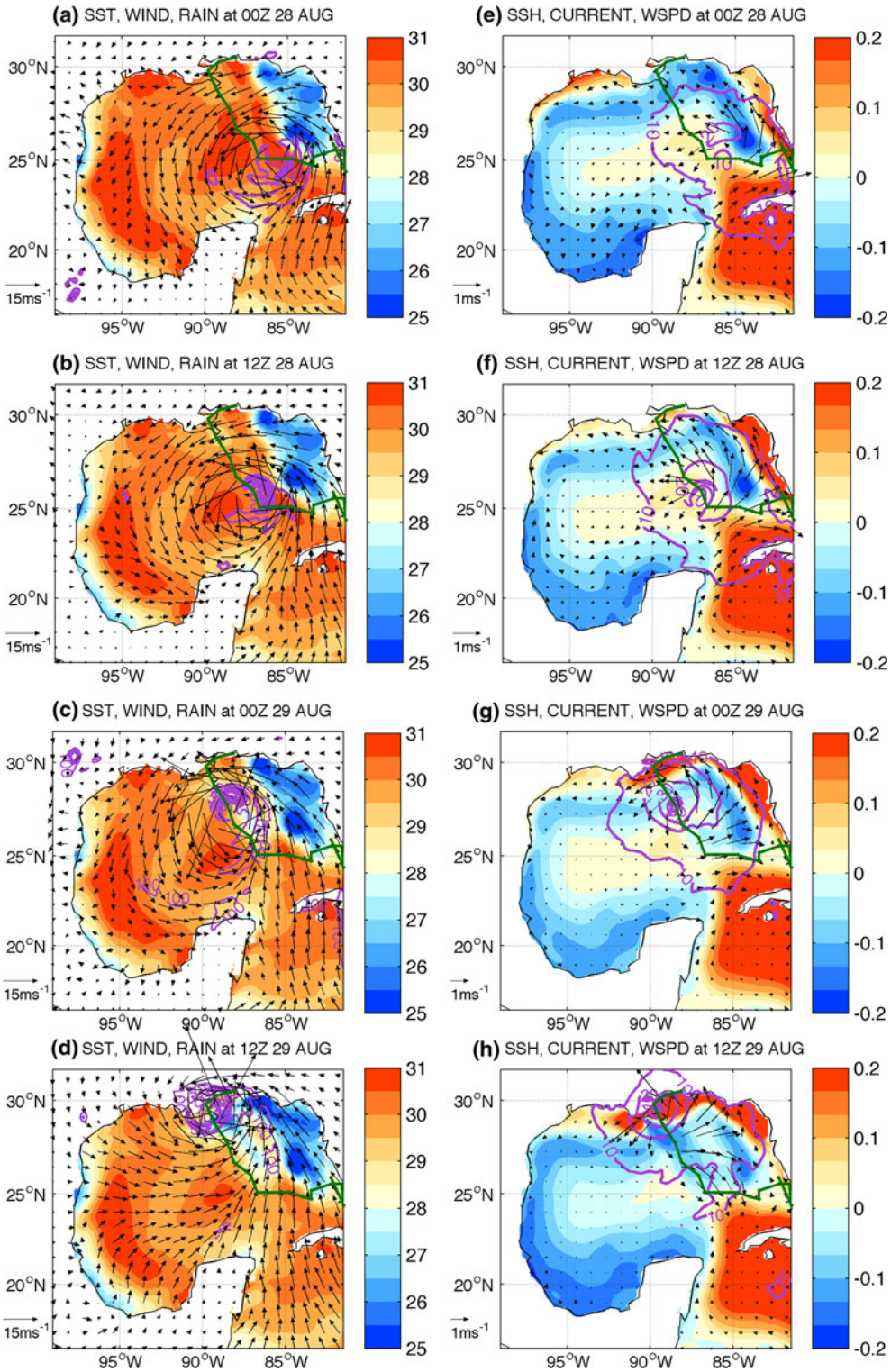

Fig. 4 Evolutions at 12-hourly intervals of *left* SST (shading, °C), 10-m wind (vectors, m s^{-1}), and rain rate (*purple contours* mm day^{-1}, CI = 200 mm day^{-1}), and *right* sea surface height (shading, m), the surface current (vectors, m s^{-1}), and 10 m wind speed (*purple contours* m s^{-1}, CI = 10 m s^{-1}) simulated from SCOAR. **a**, **e** 00Z 28 August, **b**, **f** 12Z 28 August, **c**, **g** 00Z 29 August, **d**, **h** 12Z 29 August. The reference vectors are shown in the *lower-left corner* of each panel. *Green curves* denote 6-hourly location of the minimum sea level pressure. Vectors are plotted every 7 grid points

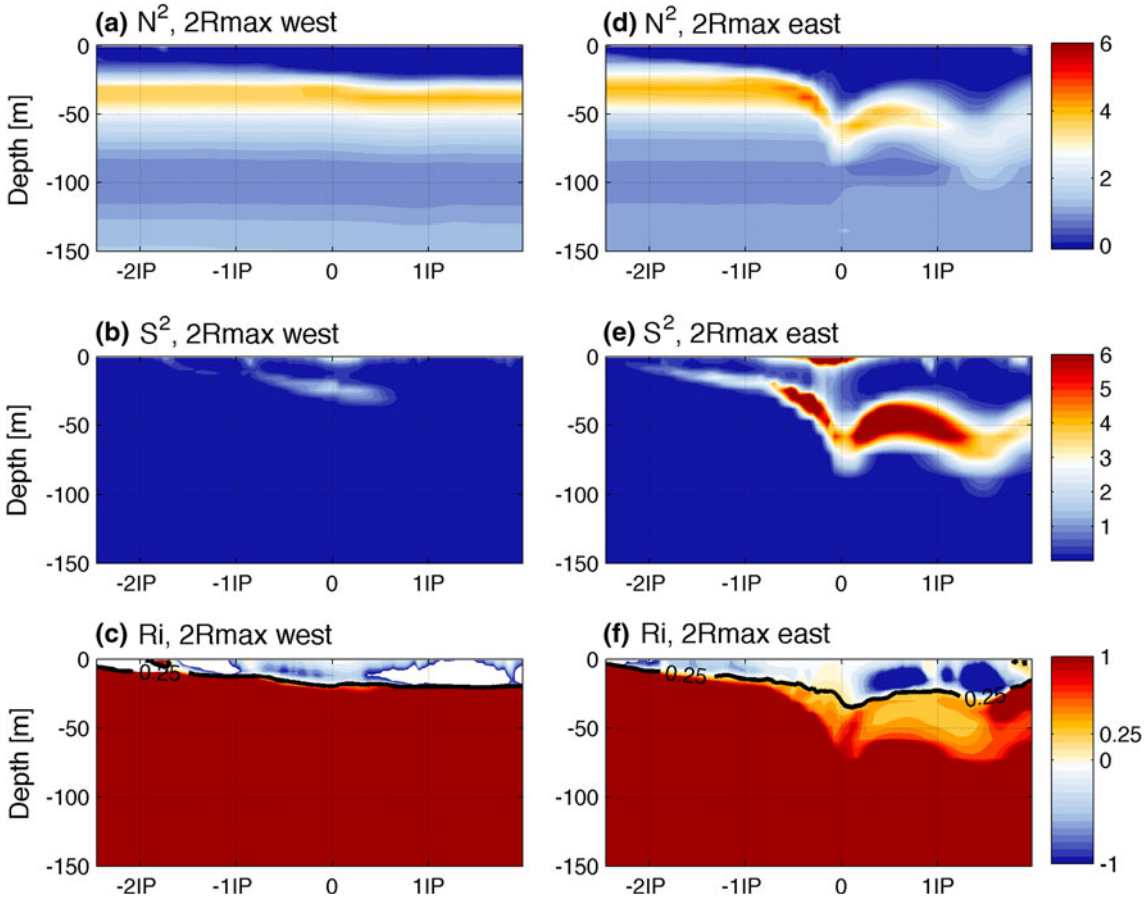

Fig. 5 Depth-time diagrams of *top* N^2 (cpd), *middle* S^2 (cpd) and *bottom* $\mathrm{Ri} = N^2/S^2$ at two locations, *left* 86.8°W, 26.5°N, and *right* 89.7°W, 26.5°N, which are located $2R_{\max}$ west and east of the reference point. The storm center passes this reference point at 18Z 28 August, which is 66 h after the initialization. $R_{\max}$ denotes the radius of the simulated maximum wind speed (~86 km). The local inertial period (IP) is 26.9 h. 0 IP marks the arrival of storm center

weaker storm in years with deeper D26 when initialized from ECCO is because D26 and thus UOHC in ECCO are not large enough to overcome the impact from the cooler SST. In other words, in the coupled model simulation with the ECCO initial condition, SST is a better predictor for the storm intensity than D26. This is further illustrated in Fig. 8 with the scatter plots of the minimum SLP with the area-averaged SST and D26 values from the initial conditions. The minimum SLP (ordinate) is obtained from the 36-h period between 18Z 27 August and 06Z 29 August (see Fig. 3) in each run. The area-averages of SST and D26 (abscissa) are made over the area in the initial conditions that overlaps the cross-track distance of $2R_{\max}$ during this 36-h period. The initial SSTs have a significant (95 %) negative correlation with the minimum SLP with the slope of the linear fit, $s = -3.68$ hPa °C^{-1}, while the D26–SLP correlation is positive with an insignificant $s = 0.14$ hPa m^{-1}. Considering that the along-track SST is a proxy for the OML dynamics and that these along-track SST and D26 variations are positively correlated (see Fig. 12 in Sect. 5), the origin of this unphysical relationship in SST/D26 with SLP is possibly due to the under-representation of mean and variability of D26 in ECCO.

To further confirm this, Fig. 9 compares interannual variability of SSH in ECCO with those from AVISO and SODA. In contrast to SODA and satellite observations, ECCO significantly underestimates the observed variability of SSH associated with the eddy shedding from the LC in GoM. D26 in ECCO is likewise much weaker than in SODA over this region. The underestimation of D26 variability in ECCO would be associated with not only the horizontal resolution but also the assimilation schemes, which use a Kalman filter-based assimilation procedure (I. Hoteit, personal communication). A more detailed examination for the causes of this underestimation is beyond the scope of the current study. Since SODA features much more realistic SSH variations compared to the satellite observations (Fig. 9c, e), the observed amplitudes of D26 variability can be inferred from those of SODA, which is ~20 m along the observed track of Katrina (88–83°W, 23–26°N).

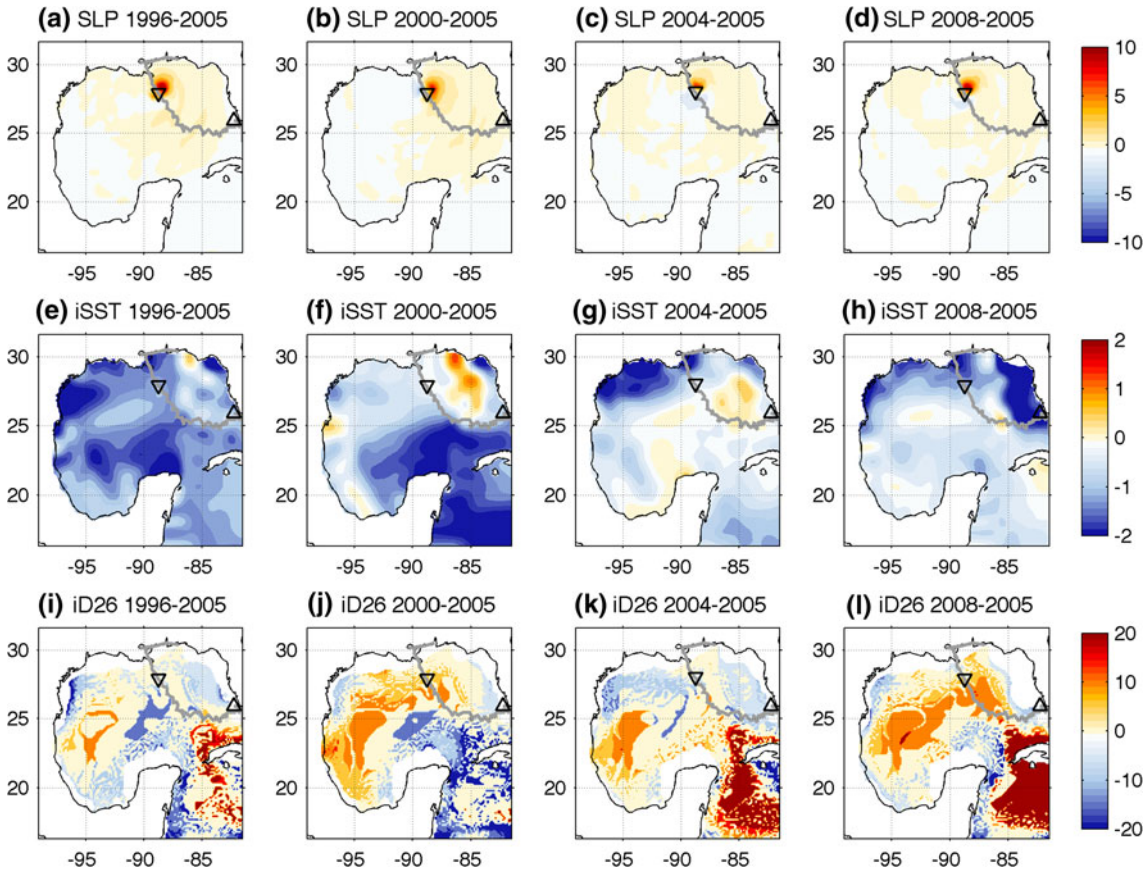

Fig. 6 **a–d** Sea level pressure (hPa) in years of 1996, 2000, 2004, and 2008 relative to 2005 at 74 h after the initialization (02Z 29 August). **e–h** as in the first row, except for the initial SST (iSST, °C) and **i–l** the initial D26 (iD26, m) relative to 2005. The *gray curves* delineate the simulated tracks of Katrina each year calculated as the location of the 1-h averaged minimum SLP, and the black curves mark the coastline of the southern Louisiana. The *red* (*blue*) shading in **a–d** indicates weaker (stronger) storm intensity compared to 2005. The *triangles* and the *inverted triangles* denote the initial time (00 h) and 74 h after the initial time, respectively

5 Sensitivity tests with modified D26

A comparison with observations in the previous sections indicates that ECCO underestimates not only the spatial structure of D26, but also its variability in GoM. In this section, a series of idealized experiments is carried out by modifying initial ECCO D26 to match the observed range to examine if a more reasonable SLP–D26 relationship can be determined.

The idealized sensitivity tests initialize the same model with the 16 ECCO initial conditions described in Sect. 4, but with the D26 variability increased to match the observed range shown in Fig. 9. This is done in the following way. The black curve in Fig. 10 denotes the profile of the temperature averaged over the region where the simulated Katrina reaches the maximum intensity (90°W–85°W, 24°N–28°N). First we identify the depth of 26 °C in each grid point, and then artificially stretched/shrank the entire water column from the identified D26 to the sea surface by 10 m and 20 m (colored curves in Fig. 10) over the entire Gulf, while keeping the surface temperature unchanged. This change in the upper layer thickness will alter the UOHC, with the difference only in subsurface thermal structure. Then, this procedure is repeated for 15 other years, and the additional sensitivity experiments are performed using them as initial and boundary conditions. Each year has thus five experiments, which are termed D20, D10, CTL, S10 and S20, where "D" ("S") denotes deepening (shoaling) throughout the study. Such an alteration of the stratification of the ocean may seem unphysical, as the resultant fields may not necessarily satisfy the geostrophy (e.g., Jacob et al. 2000). Since the stretching is applied in the entire Gulf, it is not either intended to test the impact of the realistic structure of the LC eddy on the intensity; this has been previously studied (e.g, Hong et al. 2000). By removing the limitation in D26 variability in ECCO by expanding its range of D26 variability, we intend to assess a more robust relationship between SLP and D26, which will suggest ways to improve the ECCO data assimilation procedures in representing subsurface thermal structure. As in Sect. 4, hurricane tracks in each experiment are generally insensitive to the ocean feedback, and hence we only focus on the intensity change.

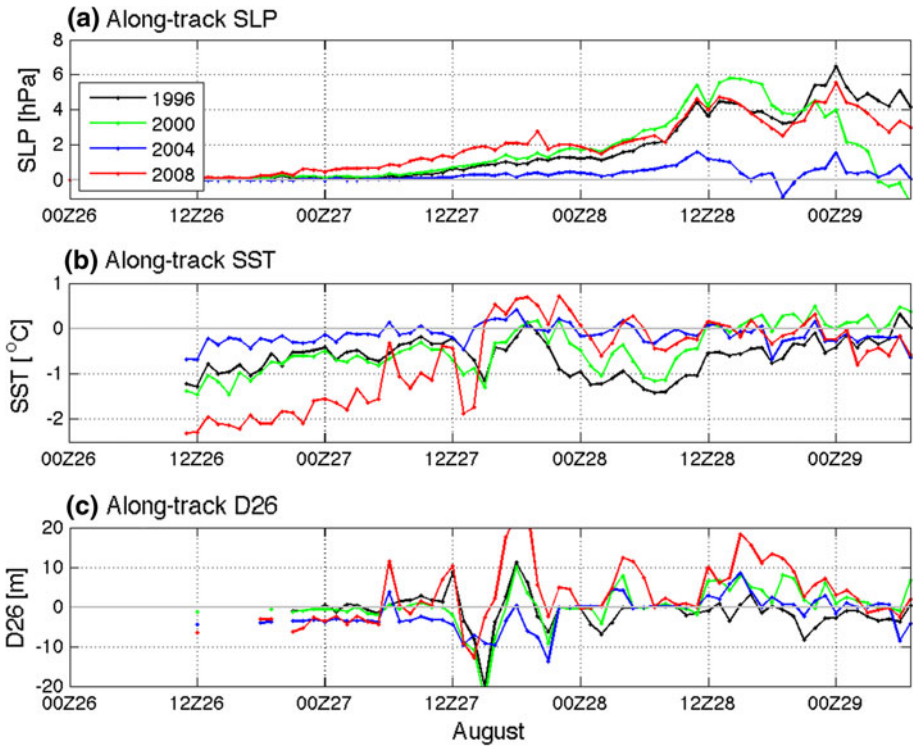

Fig. 7 The along-track evolution (1-hourly) of difference (each year—2005) in **a** SLP (hPa), **b** SST (°C) and **c** D26 (m) for the yeas of 1996, 2000, 2004, and 2008

Figure 11 shows the along-track variation SLP, SST, and θ_e in five experiments for the 2005 case. For the purpose of illustration, the deviations from the initial values are shown. The black curve is for the control case with no modification, which shows $\sim$50 hPa reduction during the evolution (Fig. 11a). SLP sensitivity to a D26 change is >20 hPa, nearly 40 % of the total 50 hPa decrease. The storm intensity is stronger for the deeper D26, as a result of the reduced along-track SST cooling (Fig. 11b, Lloyd and Vecchi 2011; Scoccimarro et al. 2011). When the initially thicker D26 is forced with the hurricane of the identical initial intensity, the hurricane-induced mixing generates less SST reduction since it needs more energy to bring the colder water from the deeper thermocline. OML dynamics play a key role in SST response under the storm center, resulting in a positive change in along-track equivalent potential temperature, θ_e, which is estimated at 1,000 hPa (Fig. 11c). The sign of $\delta\theta_e$ is directly related to the change in SLP (Malkus and Riehl 1960). As the hurricane intensifies from August 27 to 29, the difference in SST between S20 and CTL (S20 and D20) reaches more than 1.5 °C (2 °C), resulting in a change of $\delta\theta_e$ of $\sim$10 K (20 K). The differences in SST and θ_e are large enough to impact the energy production of the hurricane (Riehl 1963).

Figure 12 further illustrates the link of the altered D26 to the storm intensity, showing the scatter plots of the aforementioned variables from all 80 runs sampled following the hurricane track and then time-averaged during the intensification period before landfall. The relationship between the along-track variations in SST with D26 (Fig. 12a) clearly shows that SST change is a result of change in the upper ocean thickness of warm layer, namely, deeper the initial D26, the weaker the negative feedback. The resultant warmer inner-core SSTs over deeper D26 in turn lead to an increase in along-track θ_e (Fig. 12b), which is negatively correlated with the minimum SLP (Fig. 12c). Thus, Figs. 11 and 12 together demonstrate the regime of positive feedback between the initial thickness of the upper ocean warm layer and the intensity of Katrina via in situ OML dynamics.

Finally, Fig. 13 summarizes the relationship of the initial D26 with the intensity of Katrina. For the unperturbed D26 (black dots in Fig. 13a), initial SST is again negatively correlated with the minimum SLP with $s = -3.68$ hPa °C^{-1} (Table 1). The slope is lower for shallower D26 and greater for deeper D26, indicating a greater sensitivity of intensity to an SST with a deeper D26. The range of variation in SLP due to a 1 °C change in SST is approximately -2 to -10 hPa from S20 to D20, the latter number consistent with Sun et al. (2006). It is obvious from Fig. 13a that, for the same SST, SLP varies much more with D26, by 20 hPa for lower SST and by 30 hPa for higher SSTs. Figure 13b illustrates this D26 dependency. Each cluster of D26 of the same color shows an insignificant, or even positive, correlation with SLP variation, an incorrect relationship discussed in Sect. 4. When it is artificially amplified to match that of observations, then D26 has a significant negative correlation with the minimum SLP, with SLP variations of $\sim$30 hPa and $s = -0.68$ hPa m^{-1} (Table 1). This indicates that the

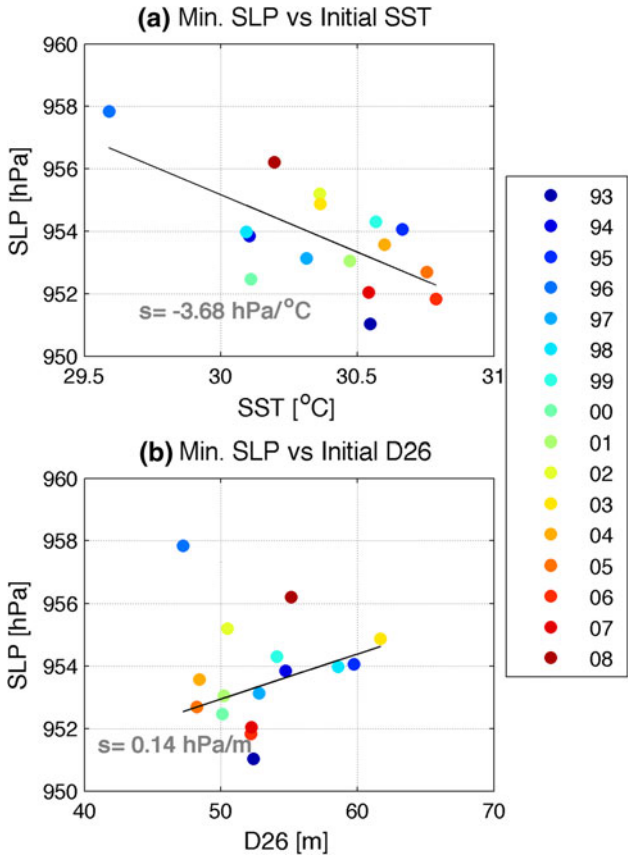

Fig. 8 The scatter plots of the minimum SLP (hPa) versus the area-averaged (**a**) initial SST (°C) and **b** initial D26 (m). The minimum SLP (*y* axis) is found from the 36 h period between 18Z 27 August and 06Z 29 August (see Fig. 3) in each run. The area-averaged initial SST and D26 values (*x* axis) are obtained by first sampling the initial conditions over the cross-track distance of $2R_{max}$ in each run, and then averaging them over the area corresponding to the 36 h period. The *straight lines* indicate the linear fit with *s* being the slope of this linear fit in unit of **a** hPa $°C^{-1}$ and **b** hPa m^{-1}. The slope in **a** is significant at 95 %, while it is no in **b**. The *different colored dots* denote the different years as shown in the legend. The year of the lowest SST (29.6 °C) in **a** is 1996

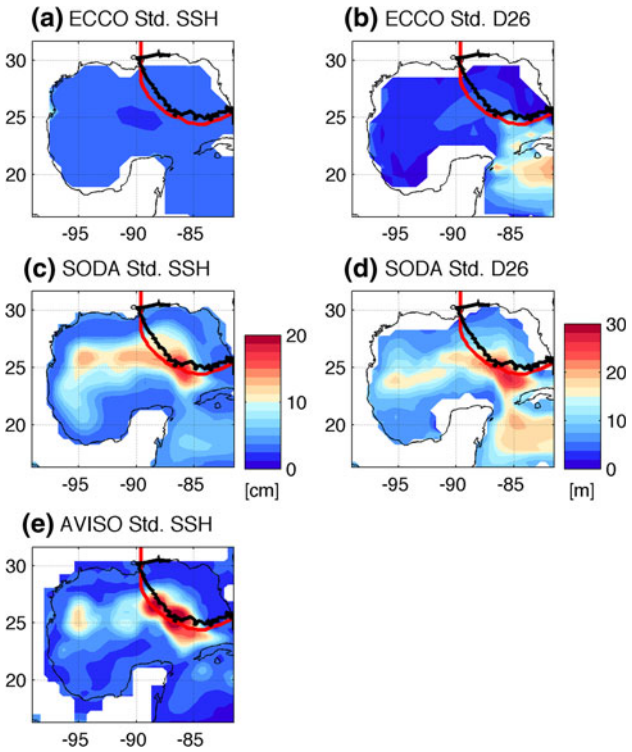

Fig. 9 Standard deviation of *left* SSH (cm) and *right* D26 (m) in *top* ECCO, **b** SODA, and *bottom* altimeter data estimated during the June–November hurricane season. The variability is estimated for the period of 1993–2008 in ECCO, and 1958–2007 in SODA, and 1993–2008 in AVISO data. The *red* (*black*) *curve* indicates the observed (simulated) track of hurricane Katrina

intensity of Katrina is determined more critically by the initial subsurface thermal structure through OML dynamics modulating θ_e, than by the initial SST. UOHC reflects both SST and D26; not only does each cluster of UOHC have an expected positive correlation with SLP with a greater slope for warmer ocean (Table 1), but also the overall scattering shows that UOHC is negatively correlated with SLP with $s = -0.28$ hPa (kJ cm^{-2}) $^{-1}$, in Fig. 13c. Figure 13 suggests that D26 is the dominant factor for UOHC and hence the intensity of Katrina.

6 Summary and discussion

Numerous studies have indicated a positive impact of subsurface thermal structure on hurricanes intensity (e.g., Schade 1994; Lin et al. 2008, 2009). As such, a more accurate knowledge of the distribution and variability of ocean thermal structure, OML dynamics, stratification, and upper ocean heat content is of fundamental importance for skillful forecast of intensity change, especially at a long forecast lead time. The active participation of the OML dynamics under the strong hurricane forcing in determining change in equivalent potential temperature in the lower atmosphere is a crucial ingredient toward improved forecasts.

This study, employing a moderate-resolution coupled regional ocean–atmosphere model initialized with the ECCO ocean state estimates for hurricane Katrina, demonstrates that hurricane–ocean interaction is sensitive to how the oceanic pre-storm subsurface thermal condition, rather than SST, is represented (Falkovich et al. 2005; Yablonsky and Ginis 2008; Halliwell et al. 2010). Result shows that the simulated intensity of Katrina is weak partly because the pre-storm D26 in ECCO is shallow. The subsurface thermal field associated with the LC and the WCRs is underestimated in ECCO having too weak spatio-temporal variations in D26. Due to this weak variability in D26, the correct relationship between storm intensity and D26 cannot be determined using initial conditions from ECCO. A series of idealized experiments

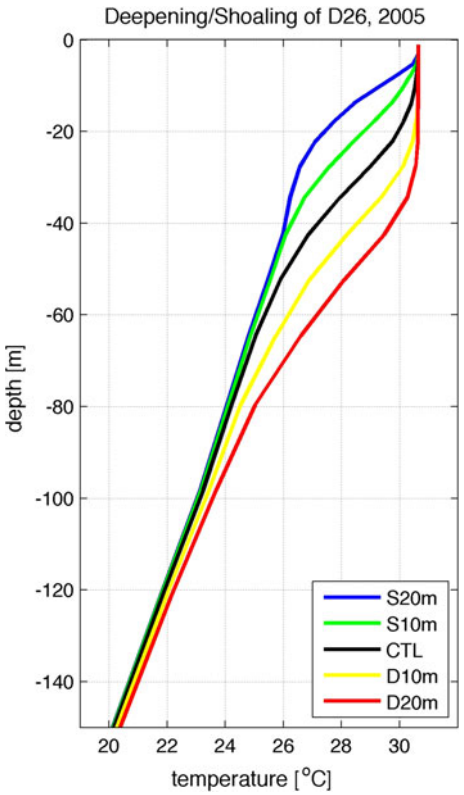

Fig. 10 Initial temperature profile on 26 August 2005 averaged over 90°W–85°W and 24°N–28°N. The *black curve* is the unaltered profiles and the *warm and cold colored curves* denote profiles with modified D26. See the text for detail

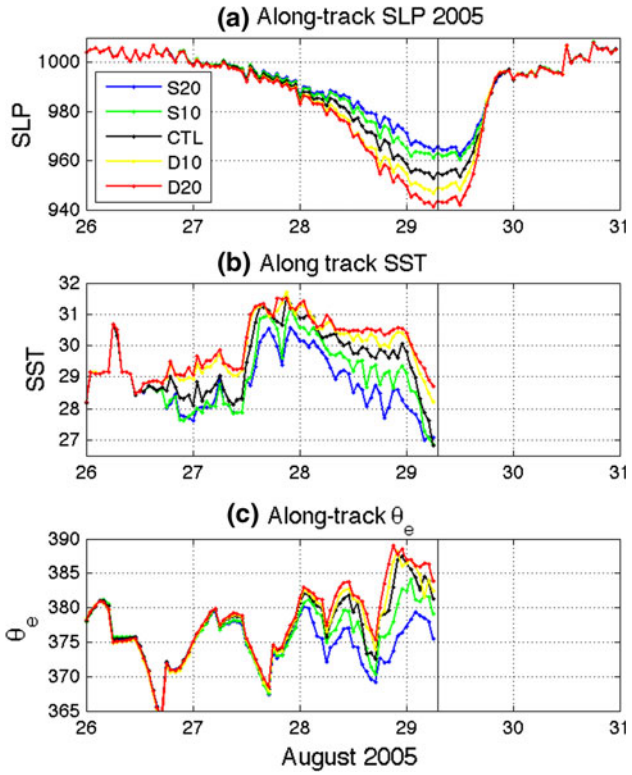

Fig. 11 **a** Time-evolution (1-hourly) of the change (δ) in along-track sea level pressure (SLP, hPa), **b** SST (°C), and **c** equivalent potential temperature (θ_e, K) at 1,000 hPa from the initial values in the five experiments for the case of 2005. *Vertical lines* denote the timing of the landfall

indicates that a more reasonable relationship between the pre-storm D26 and the intensity of Katrina is obtained when the pre-storm D26 variability is modified to match the observed range. D26 variation induces intensity change by 30 hPa, while SST generates only 12 hPa variation for the deepest D26 case. This suggests that D26 is more important for the intensification of Katrina via OML dynamics, which is corroborated in a number of studies (e.g., Shay et al. 2000; Hong et al. 2000; Emanuel et al. 2004; Goni et al. 2009). The initial subsurface fields are of great importance for the intensification in our 120-h simulations, supporting the results from the Statistical Hurricane Intensity Prediction Scheme (SHIPS) that ocean thermal structure provides a longer predictability for storm intensity (DeMaria and Kaplan 1994; DeMaria et al. 2005; Mainelli et al. 2008).

It remains challenging to accurately initialize the three-dimensional structure of the upper ocean in the hurricane coupled models. Current assimilated models, including ECCO, may not have sufficient spatial and temporal resolutions for the important small-scale structures such as the LC bulge and WCR. The fact that their spatial feature is better represented in SODA with higher horizontal resolution (0.5 °) suggests the importance of horizontal resolution. Coarse temporal resolution in ECCO (10-daily) and SODA (monthly) is, however, inadequate for the initialization of the ocean model. It should be noted that the second version of ECCO (ECCO2, Menemenlis et al. 2008) has enhanced substantially both its spatial (18 km) and temporal (daily) resolutions, leading to an improved representation of the ocean mesoscale features (e.g., Ubelmann and Fu 2011; Davis et al. 2011). How this improvement in resolutions will lead to the more reasonable relationship in D26–SLP of Katrina and other hurricanes is left as a future work. The LC variability and the associated eddy-shedding events are also known to be highly irregular with no apparent annual cycle (e.g., Vukovich 1995; Nowlin et al. 2000; Sturges and Leben 2000; Lugo-Fernández 2007). The nonlinear nature of variability in GoM subsurface thermal structure, in part caused by complex local and remote environmental forcings of varying frequencies, renders the prediction of storm intensity more arduous.

Currently, multiple satellite altimeters are blended with satellite SST measurements and in situ data to map the

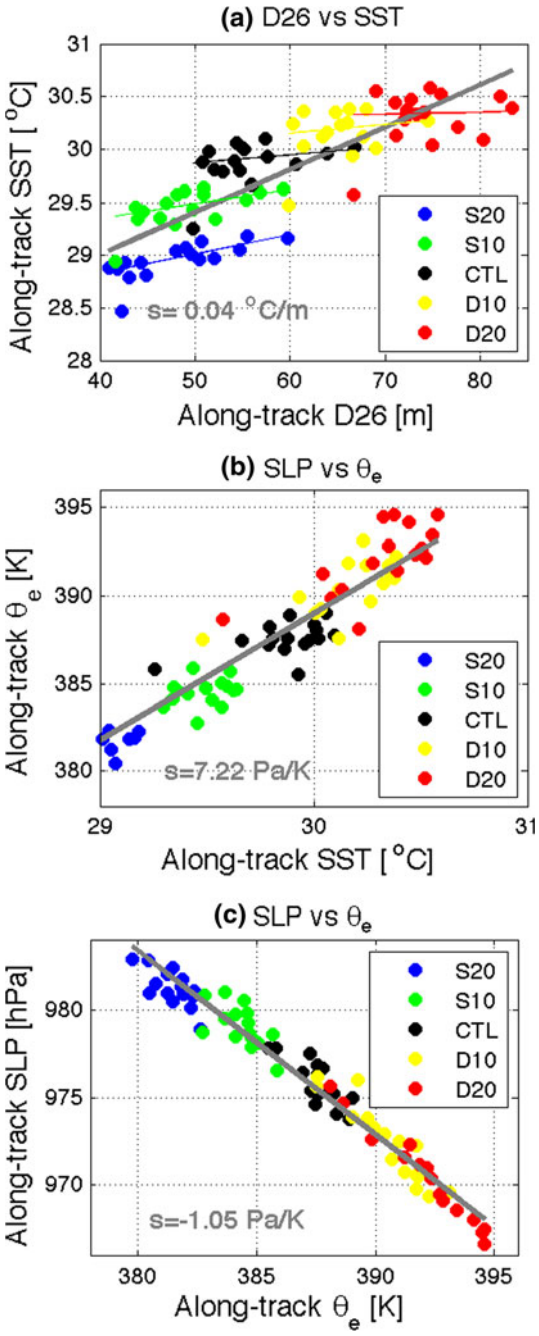

Fig. 12 Scatter plots of the along-track (**a**) SST (°C) with D26 (m), **b** θ_e (K) with SST, and **c** SLP (hPa) with θ_e from all 80 experiments. The along-track variables are averaged for the 36 h period between 18Z 27 and 06Z 29 August (before landfall). The *colored circles* indicate the experiments with different initial D26 with *red* (*blue*) being deepening (shoaling) of D26 by 10 and 20 m. The *dark* (*light*) *gray lines* denote the linear fit of the entire scatters with the slopes of linear fits displayed in each panel

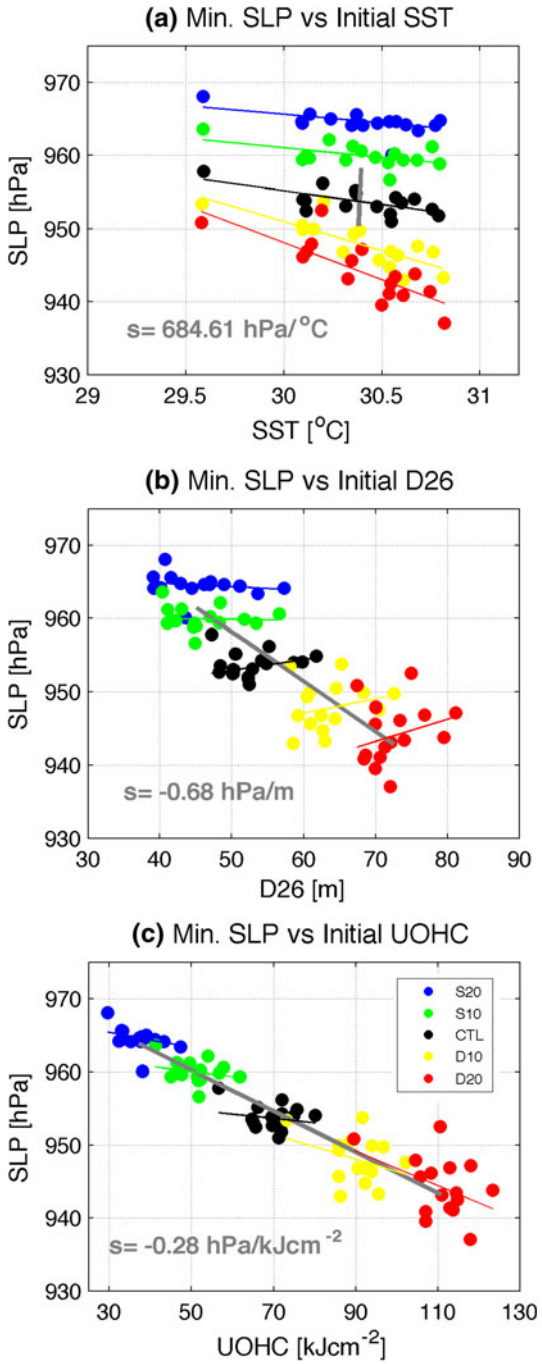

Fig. 13 **a**, **b** As in Fig. 8, except for showing the results from all 80 runs. **c** Shows the scatter plot in minimum SLP with the initial upper ocean heat content (UOHC, kJ cm^{-2}). The slopes of linear fit, s, of each cluster are summarized in Table 1. The slope $s = -0.68$ in **b** and $s = -0.28$ in **c** are significant at 99 %

eddy fields (e.g., Gilson et al. 1998; Willis et al. 2004) and infer subsurface thermal structures (Shay and Brewster 2010). This synthetic approach for the real-time monitoring of D26 and UOHC will improve our understanding of the predictability of the oceanic thermal structures (Goni et al. 2009). This has important implications as large errors still remain in hurricane intensity forecasts, and a more accurate ocean initialization can help improve intensity forecasts at a long lead-time.

Table 1 Slopes of linear fit of the minimum sea level pressure [SLP (hPa)] with the initial oceanic variables, (top) SST [°C], (middle) D26 [m], and (bottom) UOHC [kJ cm^{-2}]

Slope/runs	S20	S10	CTL	D10	D20	Total
SST (hPa $°C^{-1}$)	**−2.39**	**−2.62**	**−3.68**	**−7.94**	**−10.17**	684
D26 (hPa m^{-1})	−0.05	−0.01	0.14	0.18	0.30	**−0.68**
UOHC [hPa $(kJ\ cm^{-2})^{-1}$]	−0.10	−0.07	−0.07	−0.17	−0.24	**−0.28**

See the captions of Figs. 8 and 13 for detail. The bold faces denote the significant slopes at 95 %

Acknowledgments HS and SPX thank the support from NSF, NOAA, NASA and Japan Agency for Marine-Earth Science and Technology. HS acknowledges support from the Penzance Endowed Fund in Support of Assistant Scientists at WHOI. We thank the anonymous reviewers for their comments and suggestions, which substantially improved the manuscript.

References

Bender MA, Ginis I (2000) Real case simulations of hurricane–ocean interaction using a high resolution coupled model: Effects on hurricane intensity. Mon Weather Rev 126:917–946

Carton JA, Chepurin G, Cao X, Giese B (2000) A simple ocean data assimilation analysis of the global upper ocean 1950–95. Part I. Methodology. J Phys Oceanogr 30:294–309

Chang S, Anthes R (1978) Numerical simulations of the ocean's nonlinear baroclinic response to translating hurricanes. J Phys Oceanogr 8:468–480

Chang S, Anthes R (1979) The mutual response of the tropical cyclone and the ocean. J Phys Oceanogr 9:128–135

Cione JJ, Uhlhorn EW (2003) Sea surface temperature variability in hurricanes: implications with respect to intensity change. Mon Weather Rev 131:1783–1796

Davis X, Rothstein L, Dewar W, Menemenlis D (2011) Numerical investigations of seasonal and interannual variability of North Pacific subtropical mode water and its implications for Pacific climate variability. J Clim 24:2648–2665

DeMaria M, Kaplan J (1994) A statistical hurricane intensity prediction scheme (SHIPS) for the Atlantic basin. Weather Forecast 9:209–220

DeMaria M, Mainelli M, Shay LK, Knaff JA, Kaplan J (2005) Further improvements to the statistical hurricane intensity prediction scheme (SHIPS). Weather Forecast 20:531–543

Emanuel KA (1999) Thermodynamic control of hurricane intensity. Nature 401:665–666

Emanuel KA, DesAutles C, Holloway C, Korty R (2004) Environmental control of tropical cyclone intensity. J Atmos Sci 61:843–858

Fairall CW, Bradley EF, Rogers DP, Edson JB, Young GS (1996) Bulk parameterization of air-sea fluxes for tropical ocean-global atmosphere coupled-ocean atmosphere response experiment. J Geophys Res 101:3747–3764

Falkovich A, Ginis I, Lord S (2005) Implementation of data assimilation and ocean initialization for the coupled GFDL/URI hurricane prediction system. J Atmos Ocean Technol 22:1918–1932

Gilson J, Roemmich D, Cornuelle B, Fu LL (1998) Relationship of TOPEX/Poseidon altimetric height to steric height and circulation of the North Pacific. J Geophys Res 103:27947–27965

Goni GJ, Knaff J (2009) Tropical cyclone heat potential. Bull Am Meteorol Soc 90:S54–S56

Goni GJ, Trinanes J (2003) Ocean thermal structure monitoring could aid in the intensity forecast of tropical cyclones. EOS Trans Am Geophys Union 85:179

Goni GJ et al (2009) Applications of satellite-derived ocean measurements to tropical cyclone intensity forecasting. Oceanography 22(3):176–183

Haidvogel DB, Arango HG, Hedstrom K, Beckmann A, Malanotte-Rizzoli P, Shchepetkin AF (2000) Model evaluation experiments in the North Atlantic Basin. Simulations in nonlinear terrain-following coordinates. Dyn Atmos Oceans 32:239–281

Halliwell GR Jr, Shay LK, Uhlhorn E, Jacob SD, Smedstad O (2008) Initializing ocean models with GODAE ocean nowcast products for tropical cyclone forecasting. Mon Weather Rev 136:2576–2591

Halliwell GR Jr, Shay LK, Brewster JK, Teague WJ (2010) Evaluation and sensitivity analysis of an ocean model response to Hurricane Ivan. Mon Weather Rev 193:921–945. doi:10.1175/2010MWR3104.1

Hong X, Chang SW, Raman S, Shay LK, Hodur R (2000) The interaction of hurricane Opal (1995) and a warm core ring in the Gulf of Mexico. Mon Weather Rev 128:1347–1365

Jacob DS, Shay LK, Mariano AJ, Black PG (2000) The three-dimensional mixed layer heat balance during Hurricane Gilbert. J Phys Oceanogr 30:1407–1429

Jaimes B, Shay LK (2009) Mixed layer cooling in mesoscale eddies during Katrina and Rita. Mon Weather Rev 137(12):4188–4207

Jaimes B, Shay LK (2010) Near-inertial wave wake of hurricanes Katrina and Rita over mesoscale oceanic eddies. J Phys Oceanogr 40:1320–1337

Juang HMH, Kanamitsu M (1994) The NMC nested regional spectral model. Mon Weather Rev 122:3–26

Kain JS (2004) The Kain–Fritsch convective parameterization. An update. J Appl Meteorol 43:170–181

Kain JS, Fritsch JM (1993) Convective parameterization for mesoscale models: the Kain–Fritsch scheme. The representation of cumulus convection in numerical models, Meteor. Monogr. No. 46, Amer. Meteor. Soc. 165–170

Kanamitsu M, Ebisuzaki W, Woollen J, Yang SK, Hnilo JJ, Fiorino M, Potter GL (2002) NCEP–DOE AMIP-II reanalysis (R-2). Bull Am Meteorol Soc 83:1631–1643

Kleinschmidt E Jr (1951) Gundlagen einer Theorie des tropischen Zyklonen. Archiv fur Meteorologie, Geophysik und Bioklimatologie, Serie A 4:53–72

Knutson TR, Sirutis JJ, Garner ST, Held IM, Tuleya RE (2007) Simulation of the recent multidecadal increase of Atlantic hurricane activity using an 18-km-grid regional model. Bull Am Meteorol Soc 88:1549–1565

Kunze E (1985) Near-inertial wave propagation in geostrophic shear. J Phys Oceanogr 15:544–565

Leipper DF, Volgenau D (1972) Hurricane heat potential of the Gulf of Mexico. J Phys Oceanogr 2:218–224

Lin II, Wu CC, Emanuel KA, Lee IH, Wu CR, Pun IF (2005) The interaction of supertyphoon Maemi (2003) with a warm ocean eddy. Mon Weather Rev 133:2635–2649

Lin II, Pun IF, Ko DS (2008) Upper-ocean thermal structure and the western North Pacific category-5 typhoons. Part I. Ocean features and category-5 typhoon's intensification. Mon Weather Rev 136:3288–3306

Lin II, Pun IF, Wu CC (2009) Upper ocean thermal structure and the western North Pacific Category-5 Typhoons Part II. Dependence on translation speed. Mon Weather Rev 137:3744–3757

Lin II, Goni GJ, Knaff JA, Forbes C, Ali MM (2012) Ocean heat content for tropical cyclone intensity forecasting and its impact on storm surge. Nat Hazards. doi:10.1007/s11069-012-0214-5

Lloyd I, Vecchi G (2011) Observational evidence for oceanic controls on hurricane intensity. J Clim 24:1138–1153. doi:10.1175/2010JCLI3763.1

Lugo-Fernández A (2007) Is the loop current a chaotic oscillator? J Phys Oceanogr 37:1455–1469

Mainelli M, DeMaria M, Shay LK, Goni G (2008) Application of oceanic heat content estimation to operational forecasting of recent category 5 hurricanes. Weather Forecast 23:3–16

Malkus JS, Riehl H (1960) On the dynamics and energy transformation in steady-state hurricanes. Tellus 12:1–20. doi:10.1111/j.2153-3490.1960.tb01279.x

Menemenlis D, Campin J, Heimbach P, Hill C, Lee T, Nguyen A, Schodlok M, Zhang H (2008) ECCO2: high resolution global ocean and sea ice data synthesis. Mercator Ocean Q Newsl 31:13–21

Murakami H et al (2012) Future changes in tropical cyclone activity projected by the new high-resolution MRI-AGCM. J Clim 25:3237–3260

Nowlin WD, Jochens AE, DiMarco SF, Reid RO (2000) Physical oceanography. Deepwater Gulf of Mexico environmental and socioeconomic data search and synthesis, vol 1. Narrative Report, OCS Study MMS 2000-049, Gulf of Mexico OCS Regional Office, Minerals Management Service, U.S. Department of the Interior, New Orleans, LA, pp 61–121

Powell MD, Houston SH, Reinhold TA (1996) Hurricane Andrew's landfall in South Florida. Part I: standardizing measurements for documentation of surface wind fields. Weather Forecast 11:304–328

Price JF (1981) Upper ocean response to a hurricane. J Phys Oceanogr 11:153–175

Price JF (2009) Metrics of hurricane–ocean interaction. Vertically-integrated or vertically-averaged ocean temperature? Ocean Sci 5:351–368

Price JF, Sanford TB, Forristall GZ (1994) Forced stage response to a moving hurricane. J Phys Oceanogr 24:233–260

Reynolds RW, Smith TM, Liu C, Chelton DB, Casey KS, Schlax MG (2007) Daily high-resolution blended analyses for sea surface temperature. J. Clim 20:5473–5496

Riehl H (1963) Some relations between wind and thermal structure of steady state hurricanes. J Atmos Sci 20:276–287

Riehl H, Malkus JS (1961) Some aspects of Hurricane Daisy, 1958. Tellus 13:181–213

Sanford TB, Black PG, Haustein J, Fenney JW, Forristall GZ, Price JF (1987) Ocean response to hurricanes, Part I. Observations. J Phys Oceanogr 17:2065–2083

Sanford TB, Price JF, Girton JB, Webb DC (2007) Highly resolved ocean response to a hurricane. Geophys Res Lett 34:L13604

Schade LR (1994) The ocean's effect on hurricane intensity. Ph.D. thesis, Massachusetts Institute of Technology, USA

Schade LR, Emanuel KA (1999) The ocean's effect on the intensity of tropical cyclones: results from a simple atmosphere-ocean model. J Atmos Sci 56:642–651

Scharroo R, Smith WH, Lillibridge JL (2005) Satellite altimetry and the intensification of Hurricane Katrina. EOS 86:366–367

Scoccimarro E et al (2011) Effects of tropical cyclones on ocean heat transport in a high-resolution coupled general circulation model. J Clim 24:4368–4384

Seo H, Miller AJ, Roads JO (2007) The Scripps Coupled Ocean–Atmosphere Regional (SCOAR) model, with applications in the eastern Pacific sector. J Clim 20:381–402

Shay LK (2009) Upper ocean structure: a revisit of the response to strong forcing events. In: Steele J et al (eds) Encyclopedia of ocean sciences, pp 4619–4637. Elsevier Press, Amsterdam

Shay LK, Brewster JK (2010) Oceanic Heat Content Variability in the Eastern Pacific Ocean for Hurricane Intensity Forecasting. Mon. Wea. Rev. 138:2110–2131

Shay LK, Uhlhorn EW (2008) Loop Current response to Hurricanes Isidore and Lili. Mon. Wea. Rev. 136:3248–3274

Shay LK, Goni GJ, Black PG (2000) Effect of a warm oceanic feature on hurricane Opal. Mon. Wea. Rev. 128:1366–1383

Shchepetkin AF, McWilliams JC (2005) The regional oceanic modeling system (ROMS): a split-explicit, Free-surface, topography-following-coordinate ocean model. Ocean Modell. 9:347–404

Sturges W, Leben R (2000) Frequency of Ring Separations from the Loop Current in the Gulf of Mexico: A Revised Estimate. J Phys Oceanogr 30:1814–1819

Sun D, Gautam R, Cervone G, Boybei Z, Kafatos M (2006) Comment on Satellite altimetry and the intensification of Hurricane Katrina. EOS Trans. AGU 87(8):89

Sutyrin GG, Khain AP (1984) On the effect of air–ocean interaction on the intensity of a moving tropical cyclone. Atmos Ocean Phys 20:787–794

Ubelmann C, Fu L (2011) Cyclonic eddies formed at the Pacific tropical instability wave fronts. J Geophys Res 116:C12021

Vukovich FM (1995) An updated evaluation of the loop current eddy-shedding frequency. J Geophys Res 100(C5):8655–8659

Wang Y (1998) On the bogusing of tropical cyclones in numerical models: the influence of vertical structure. Meteorol Atmos Phys 65:153–170

Weller RA (1982) The relation of near-inertial motions observed in the mixed-layer during the JASIN (1978) experiment to the local wind stress and to the quasigeostrophic flow field. J Phys Oceanogr 12:1122–1336

Willis JK, Roemmich D, Cornuelle B (2004) Interannual variability in upper ocean heat content, temperature, and thermosteric expansion on global scales. J Geophys Res 109:C12036

Willoughby HE, Black PG (1996) Hurricane Andrew in Florida. Dynamics of a disaster. Bull Am Meteorol Soc 77:543–549

Wu CC, Lee CY, Lin II (2007) The effect of the ocean eddy on tropical cyclone intensity. J Atmos Sci 64:3562–3578

Yablonsky RM, Ginis I (2008) Improving the initialization of coupled hurricane–ocean models using feature-based data-assimilation. Mon Weather Rev 136:2592–2607

Yoshimura K, Kanamitsu M (2008) Dynamical global downscaling of global reanalysis. Mon Weather Rev 136:2983–2998

Zamudio L, Hogan PJ (2008) Nesting the Gulf of Mexico in Atlantic HYCOM: oceanographic processes generated by Hurricane Ivan. Ocean Model 21:106–125

Zhao M, Held IM, Lin S-J, Vecchi GA (2009) Simulations of global hurricane climatology, interannual variability, and response to global warming using a 50-km resolution GCM. J Clim 22:6653–6678

Zedler SE, Dickey TD, Doney SC, Price JF, Yu X, Mellor GL (2002) Analyses and simulations of the upper ocean's response to Hurricane Felix at the Bermuda Testbed Mooring site. J Geophys Res 107(C12):3232. doi:10.1029/2001JC000969